PCCP

Resistive Switching Properties of Epitaxial BaTiO3-δ Thin Films Tuned by After-Growth Oxygen Cooling Pressure

Journal Name

ARTICLE

Resistive Switching Properties of Epitaxial BaTiO$_{3-\delta}$ Thin Films Tuned by After-Growth Oxygen Cooling Pressure

Yooun Heo[a], Daisuke Kan[b], Yuichi Shimakawa[b, c] and Jan Seidel*[a]

BaTiO$_{3-\delta}$, i.e. oxygen-deficient barium titanate (BaTiO$_3$), thin films grown on GdScO$_3$ (110) substrates with SrRuO$_3$ conductive electrodes by pulsed laser deposition are studied by X-ray diffraction and conductive AFM to characterize their structure and nanoscale electronic properties. Bias and time-dependent resistive switching measurements reveal a strong dependence on oxygen vacancy concentration, which can be tuned by after-growth oxygen cooling conditions of the thin films. Results indicate that resistive switching properties of BaTiO$_{3-\delta}$ can be enhanced by controlling oxygen deficiency and provide new insight for potential non-volatile resistive random-access memory (RRAM) applications.

1 Introduction

Barium titanate (BaTiO$_3$) is well known as a promising ferroelectric material with a high dielectric constant and superior chemical stability that is widely used in actuator and sensor devices.[1-3] Considerable research efforts have been made to investigate the suitability of BaTiO$_3$ for storage applications based on e.g. tunnel junction concepts[4-8] and resistive switching, which is usually observed in capacitor-like structures consisting of various metal oxides including multi-elemental perovskite-type oxides[9-12] and binary oxides.[13-17] The observed resistive switching mechanisms and behaviours are diverse and some possible scenarios have been proposed. Two broad types can be considered to classify these mechanisms in terms of microscopic physics. One is based on ionic movement[18] or the formation of conductive filaments and channels, e.g. through local redox reactions. Another interface driven mechanism is based on electromigration of oxygen vacancies,[19] which induces a change in the valence states of cations in the metal oxide, resulting in a change in the electronic states and thus alteration of conductivity. Despite intensive studies on RRAM concepts, the exact switching mechanism based on physical analysis for various materials is not fully investigated yet. Since the very first report of a resistive switching effect in ferroelectric niobium oxide[20], much attention has been given to ferroelectric perovskite titanates[21-24]

in the study of ferroelectric resistive switching. In addition to these studies of driving mechanisms, the aspect of engineering of thin films and structures was also investigated in ferroelectric perovskite titanates, e.g. Cr-doped (Ba, Sr)TiO$_3$[10], and BaTiO$_3$ films with an electrode of La$_{0.7}$Ca$_{0.3}$MnO$_3$.[25] More recently, the temperature dependence of *I-V* characteristics in BaTiO$_3$/La$_{0.8}$Ca$_{0.2}$MnO$_3$ was reported, showing diode-like asymmetric characteristics below 250K and resistive switching behaviour at higher temperature.[26] As such, there has been a vast amount of effort to exploit the potential of materials in various aspects of their functional properties. Among the various models proposed for resistance switching, the oxygen migration based model has attracted much attention due to the notable demonstration of switching behaviours at the Pt/TiO$_2$ interface.[27-32] In many oxide systems, oxygen vacancies behave as mobile donors[33-35] and electrical control of their concentration at the metal/oxide interface is attractive for memory applications if tuning and strict control of oxygen content is possible.

In this paper, we report on well-defined resistive switching properties of oxygen deficient epitaxial BaTiO$_{3-\delta}$ films fabricated with defined after-growth oxygen cooling conditions by using nanosize electric characterization via conductive AFM (c-AFM) at room temperature. Unlike previous studies on switchable diodes, we used several oxygen deficient films of barium titanate as a switching element, since their electrical conductivity can be controlled simply by an additional post cooling process, i.e. annealing in a defined oxygen environment, resulting in a modulation of the oxygen vacancy concentration. Current-voltage behaviour from I-V curve measurements show that the current magnitude is strongly dependent on oxygen vacancy content in the films, providing a clue to the mechanism involved. Bias and time-dependent I-V

[a.] School of Materials Science and Engineering, University of New South Wales, Sydney, NSW 2052, Australia E-mail: jan.seidel@unsw.edu.au
[b.] Institute for Chemical Research, Kyoto University, Gokasho, Uji, Kyoto, 611-0011, Japan
[c.] Japan Science and Technology Agency, CREST, Uji, Kyoto 611-0011, Japan
†Electronic Supplementary Information (ESI) available: AFM topography scans, Fitting of *I-V* curves to Schottky model and *I-V* curve measurements over a period of time. See supporting information

curve measurements show that resistance switching properties can be tuned by varying amplitude and time duration of applied bias as means to control the device properties in the system. $BaTiO_{3-\delta}$ films with large amounts of oxygen vacancies exhibit clear rectifying *I-V* characteristics and hysteretic behaviour. The large discrepancy observed between the onset voltage of electrical current starting to flow and the coercive voltage required for ferroelectric switching suggests that the ferroelectric contribution to resistive switching is rather small for samples containing considerable amounts of oxygen vacancies. Instead, our results reveal that the local distribution of oxygen vacancies and their bias dependent movement play a crucial role in the emergence of the resistive switching effect. Furthermore, resistive switching characteristics in pulse-voltage mode are presented to evaluate the repeatability and potential for device applications.

2. Experimental methods

2.1 Sample Preparation

60 nm thick oxygen deficient barium titanate $BaTiO_{3-\delta}$ (BTO) films were epitaxially grown by pulsed laser deposition on $GdScO_3(110)_o$(GSO) substrates capped by a 10-15 nm-thick $SrRuO_3$(SRO) layer that served as a bottom electrode[36] at 700°C (The subscripts *o* denote the orthorhombic perovskite notation). GSO (a_o=5.49 Å, b_o=5.75 Å, c_o=7.93 Å) has a closely matched in-plane lattice parameter to BTO ($a = b = 3.99$ Å, $c = 4.04$ Å) with bulk lattice mismatch strain of 0.67%. The BTO layer was deposited from a sintered ceramic stoichiometric BTO target using a KrF excimer laser (λ=248 nm) at 1.5 J/cm^2 and 2Hz repetition rate. For the deposition of the SRO layer, the Ru-rich $SrRu_{1.1}O_3$ target was used to minimize possible Ru deficiencies and was pulsed at 1.0 J/cm^2. The oxygen pressure during the BTO and SRO deposition was set to be 25 and 100 mTorr, respectively. To vary the amount of oxygen vacancies in the BTO layer, the deposited films were cooled under various oxygen pressures ranging from 50 µTorr to 100 Torr.[37, 38] Controlling the amount of oxygen vacancies and their distribution can be used to tune the conductivity in perovskite oxides.[39-41]

2.2 Characterizations of Structural and Physical Properties

The crystal structure and thin film orientation were analyzed by a conventional four-circle diffractometer (PANalytical X'PertMRD) at Kyoto University. A commercial scanning probe microscope system (AIST-NT SmartSPM) was used to perform the measurements of c-AFM and PFM at UNSW. A conductive diamond coated tip with a force constant of around 40-50N/m (DCP20, NT-MDT) was used for imaging and *I-V* curves. For pulsed mode measurements, the voltage pulses and current reading for resistive switching were monitored by a built-in oscilloscope in SmartSPM.

3. Results and discussion

Atomic force microscopy (AFM) images show that our PLD-grown samples have smooth surface morphology with root-mean-square (rms) surface roughness around 0.25nm as shown in the supplementary information (Fig. S1). No obvious protruding surface features were observed in the samples, indicating a two dimensional growth of the BTO layer.[24] Figure 1a shows $2\theta-\theta$ profiles around the $(220)_o$ GSO Bragg reflection for the films grown with various oxygen cooling pressures ranging from 50 µTorr to 100 Torr. The films only show the (002) BTO reflection and $(220)_o$ SRO reflections without any reflections from impurity phases, confirming the epitaxial growth of the films on the GSO substrate. We also performed X-ray reciprocal space maps (RSMs). Figure 1b displays the semi-logarithmic contour plot of the RSM around the $(444)_o$ GSO Bragg reflection for the films prepared by cooling under an oxygen pressure of 25 mTorr. The (103) BTO, $(444)_o$ SRO and $(444)_o$ GSO reflections are seen at the same position along the horizontal axis, indicating that the in-plane lattices of BTO and SRO are fixed by the substrate. Essentially the same results are seen for all fabricated films. The (103) BTO reflection position along the vertical axis, which corresponds to the out-of-plane direction of the BTO layer, remains almost unchanged with the oxygen cooling pressure. The independence of the lattice parameter of the BTO layer on the oxygen cooling pressure is also confirmed from Figure 1a which shows that the (002) BTO reflections for all the films appear at the same 2θ position. We also note that the full width at half maximum (FWHM) of the (002) BTO reflection shows no obvious dependence on cooling pressure and remains as small as ~0.07°. This ensures the high quality of the fabricated BTO film layer regardless of the amount of oxygen vacancies.

Current–voltage characteristics and resistive switching behaviour of BTO films were measured with an AIST-NT SmartSPM in c-AFM mode. Electrical bias was applied through the sample with the tip grounded for all the measurements shown in Figure 2. With the start and end of the bias sweep set to 0V, by sweeping the bias from negative to positive, typical
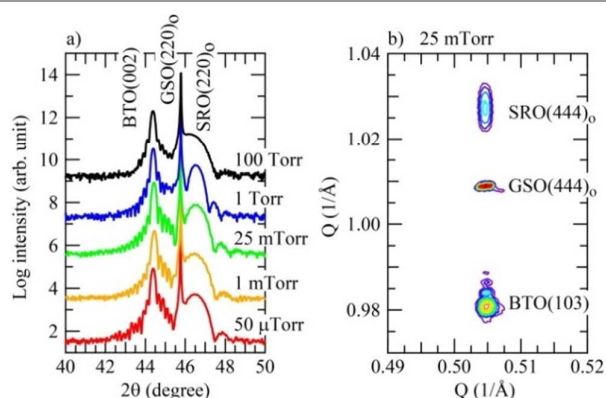

Figure 1. XRD study of various oxygen deficient BTO thin films: (a) $2\theta-\theta$ profiles for the $BaTiO_{3-\delta}$ films grown under varying oxygen cooling conditions. (b), Semi-logarithmic contour plot of reciprocal space mapping around the $(444)_o$ $GdScO_3$ (GSO) Bragg reflection for the 25 mTorr sample (similar RSM maps were obtained for other samples). The reflections from SRO and GSO are indexed using an orthorhombic unit cell.
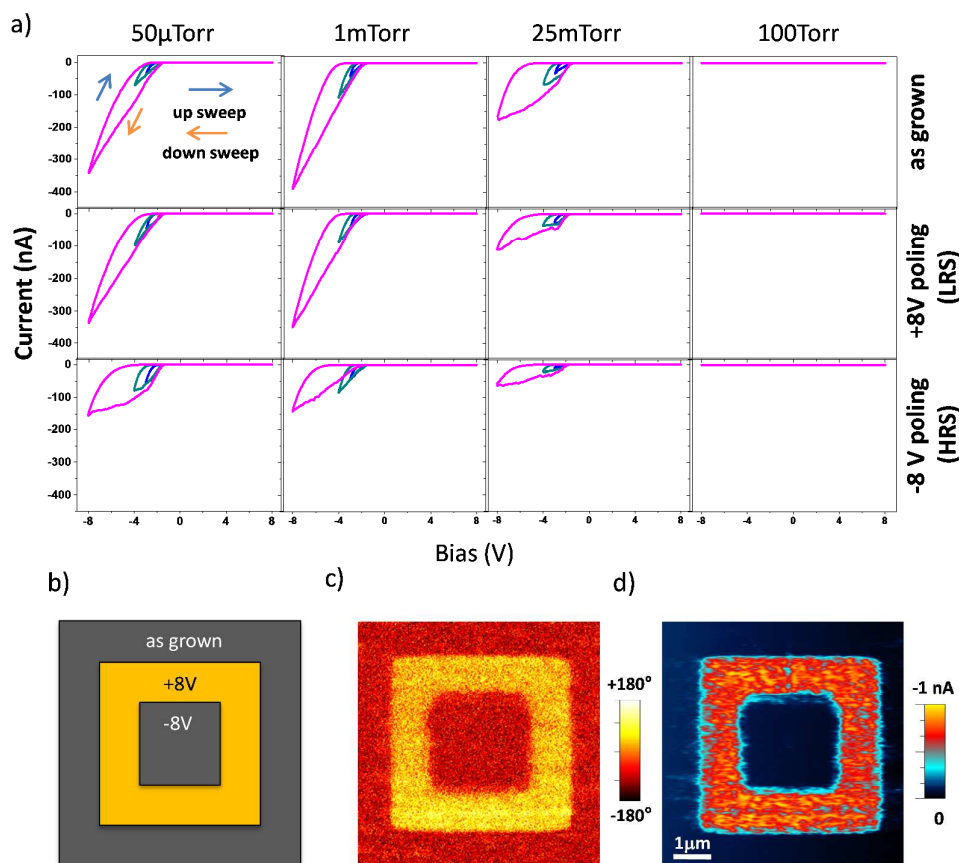
Figure 2. PFM and c-AFM study of various BTO films. (a) Locally acquired *I-V* curves of resistive switching behaviour for various BTO films in as-grown and different pre-poled areas with *I-V* end-voltages of -3V (blue), -4V(green), and -8V(violet). (b) Schematic of applied poling voltages for BTO films. (c and d) Piezoresponse (PFM) phase image indicating ferroelectric polarization in +8V area has been switched (polarization: yellow -up, brown -down) and c-AFM image at -2V bias (low bias) showing resistive switching behaviour of poled area for the 50 µTorr sample.

current-voltage (*I-V*) characteristics of as-fabricated BTO films cooled under different oxygen cooling pressures are shown in top panels in Figure 2a. As can be seen, the *I-V* characteristics are strongly dependent on the oxygen cooling pressure. Very low currents of few pA just above the detection limit (~0.2pA) are observed for the film cooled under the largest pressure (100 Torr, see also supplementary information) as shown in Fig. S2 and similar properties are seen for samples cooled under an oxygen pressure of 1 Torr and larger. For samples cooled at lower oxygen pressure the current under negative bias is drastically increased. By comparing the current of each sample, read at the end voltages during the sweep, we find a close relation between the electrical conductivity and the after-growth oxygen cooling pressure, considering that the conductivity of the film cooled at 50 µTorr is substantially enhanced with its current read at -8V being more than 4 orders of magnitude greater than that of the sample cooled at 100 Torr. These results show a clear relation between overall conductivity of the film and the oxygen cooling pressure and provide a clue to control electronic properties of $BaTiO_{3-\delta}$. We attribute the

conduction mechanism to oxygen vacancies created within the films from the after-growth cooling process. However, quantitative determination of the oxygen vacancy concentration in the films was difficult because the film's resistance (along the in-plane direction) was too large and this did not allow for Hall resistivity measurements. Raman analysis could potentially be employed to see structural and compositional changes for characterising the variation of oxygen vacancies although quantitative evaluation is still uncertain in our system.[42] Nonetheless, the AFM based *I-V* curves exhibit a clear rectifying characteristic and hysteretic behaviour with two different reading currents at the same voltage for up and down bias sweep,[43] therefore representing two resistance states, which has been observed before in c-AFM measurements on ferroelectric oxides.[44] As seen in the middle and the bottom panels of *I-V* curves, poled by +8 and -8V respectively in Fig. 2, the electrical conductivity can be modulated by electric field such that positive bias switches the BTO film to a low resistance state (LRS), whereas the negative bias reversely switches the BTO back to high resistance state (HRS).

Regardless of poled states however, the current is found to start increasing at around 1.3V (current onset, i.e. current above the detection limit (~0.2pA) of the c-AFM setup). In fact, the observation of rectifying characteristics suggests the formation of interfacial barriers in the system.

To further analyse the electrical behaviour of the samples, the current-voltage curves are plotted on a semi-logarithmic scale and a representative log I-V curve of the 50 μTorr sample is shown in the supplementary information (Fig. S3). The I-V curves in the low voltage region for both LRS and HRS during up and down sweep respectively, are well-fitted to a straight line. This result agrees with a basic Schottky barrier conduction model, meaning that the thermionic emission process is predominant. The ideality factors, n, of LRS and HRS based on the I-V curves by using a thermionic emission model are roughly 5 and 11, respectively, for the sample cooled at 50 μTorr (see Supporting Information). While this is much larger than the ideal value of 1 in a semiconductor Schottky junction, such a large ideality factor has been reported in other switchable diodes[45] and the metal/porous-Si/Si diodes.[46] In the case of the metal/porous-Si/Si diode, the rectifying behaviour stems from the band bending inside the Si layer at the interface and the porous Si layer acts as a barrier to the carrier conduction. The large series resistance due to the porous-Si layer results in the large ideality factor of the metal/porous-Si/Si diode. With this in mind, the large n values in our samples can be attributed to an additional barrier layer that may form between the tip and $BaTiO_{3-\delta}$. Further work by cross-sectional TEM characterisations can be used to observe this additional layer.[47] Considering that the thermionic emission process dominates the conduction mechanism in the probed region, the resistive switching behaviour of BTO films is attributable to Schottky barrier modulation with oxygen vacancy migration. For example, the larger currents in the LRS are owing to a reduced barrier height with larger distribution of oxygen vacancies with respect to the HRS. This observation indicates that oxygen vacancies in the BTO films, which provide electronic carriers, play an important role in the observed electronic properties of the material.

In order to understand and visualize the conductivity after switching with different set-voltages, we pre-poled the films in micron sized areas as shown schematically in Figure 2b. Piezoresponse (PFM) and c-AFM images after pre-poling are acquired for the 50 μTorrFigure 2c shows that the ferroelectric polarization has been switched in the area where +8V was applied and switched back in the inner area with -8V bias. Such ferroelectric switching behaviour is observed by PFM scans in all of the BTO films. Increased conductivity is seen during the c-AFM scan at "read" bias voltage of -2V in Figure 2d. The region with polarization reversal to the downward direction remains highly conductive in comparison to the as-grown region and the region poled with -8V. After applying a poling voltage of around ±3V in a 4-by-4μm^2 area, exceeding the coercive voltage, the switching of ferroelectric domains is observed with a clear phase contrast (~180°). In fact, this

minimal voltage required for the ferroelectric switching is much greater than the observed onset voltage range for the current in the I-V curves during the bias down-sweep in Figure 2. We also compared the onset voltages of current flow between the samples grown at different cooling oxygen pressures and poling states, however, no clear relation was found. It is important to note that in the I-V curves there is no apparent change in current associated with the ferroelectric switching around its coercive voltage. These observations indicate that while the data in Figure. 2c and 2d would suggest a correlation between the ferroelectric polarization direction and the current, the contribution of polarization reversal to the change of electrical conductivity is rather small. Instead, we can explain the resistive switching mechanism in terms of distribution of oxygen vacancies along with modulation of interfacial barriers. In our system, the nano-capacitor structure, consisting of diamond tip/$BaTiO_{3-\delta}$/SRO suggests the formation of a Schottky-like barrier, considering the rectifying I-V characteristics and the bias direction. However, the interface of $BaTiO_{3-\delta}$/SRO also forms a Schottky barrier that can be modulated by ferroelectric polarization, resulting in hysteretic and rectifying charactersitics.[48] Provided that the oxygen vacancies are positive charge carriers that can be tuned by electrochemical interaction,[49] the application of the positive bias accumulates the oxygen vacancies near the top surface and leads to a highly conductive surface layer (with low-valent Ti), resulting in LRS, while the applied negative bias dispreads the vacancies from the surface region and forms an insulating surface layer (with high-valent Ti), resulting in HRS, as shown in Fig. 3. With this in mind, the interfacial effect at the diamond tip/$BaTiO_{3-d}$ interface should dominate the conduction mechanism. Therefore, the bias dependent oxygen vacancy
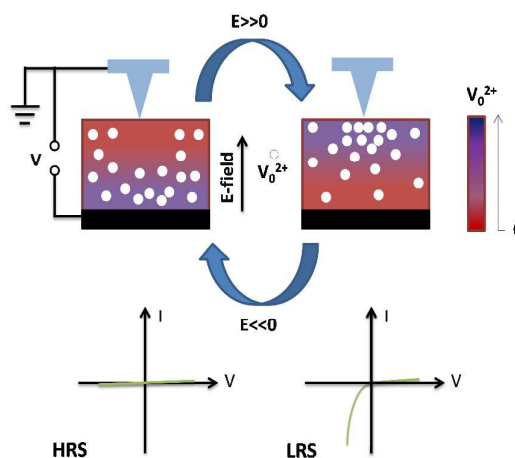

Figure 3. The mechanism of the bias-dependent movement of oxygen vacancies. Schematic diagram illustrating the electric field dependent movement of oxygen vacancy (Vo2+), which results in the change in the distribution of the Vo2+ contents in $BaTiO_{3-\delta}$ films. Oxygen vacancies are spontaneously produced during the sample cooling process and respond to electric field because the oxygen vacancies are positively charged. In a positive field (from bottom to top directional field), oxygen vacancies are moving upward and accumulating near the top surface. By applying opposite bias voltage, and thus the negative electric field, the oxygen vacancies can be dispersed from the top surface. Consequently, I-V curves are dependent on the oxygen vacancy contents that can be tuned by bias voltage.

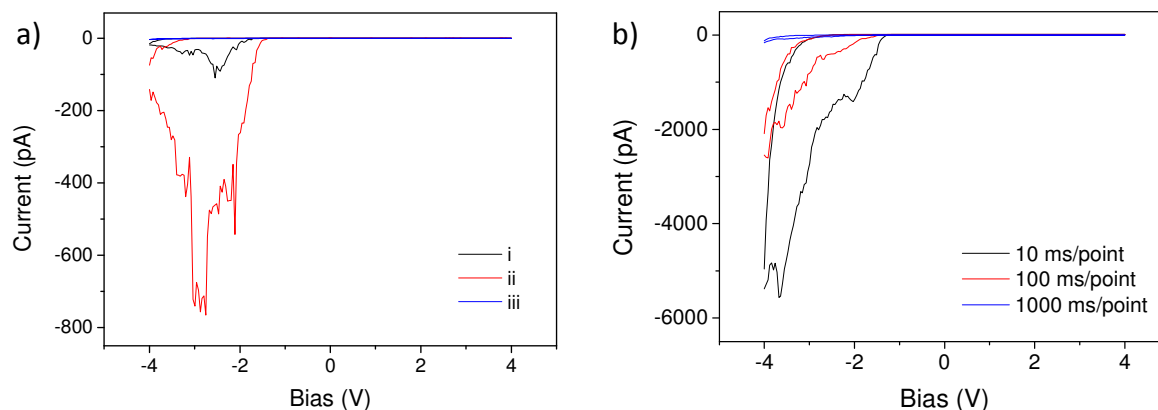Please do not adjust margins

Journal Name

ARTICLE

Figure 4. *I-V* curve measurements for different poling history and time dependent studies of resistive switching behaviour for the 50 µTorr sample. (a) *I-V* curves for different poling history at ramping speed of 100ms/point: i) Normal *I-V* curve (-4V to +4V), ii) *I-V* curve (-4V to +4V) after taking an *I-V* curve (0V to +8V), iii) *I-V* curve (-4V to +4V) after taking a *I-V* curve (0V to -8V). (b)) *I-V* curves up to 4V bias with different bias ramping speeds (200 points per curve) after pre-poling with +8V. High speed (the 10ms/point scan) retains increased current levels set by pre-poling positive bias with +8V while slow speeds show highly decreased current levels at -4V due to neutralizing of the positive voltage pre-poling.

movement should play a decisive role for the resistance switching in the oxygen deficient BTO films. In fact, this bias-dependent oxygen vacancy movement in turn, results in the modulations of the local resistance.[50]

We also measured *I-V* curves over a long period of time to directly see the impact of oxygen vacancies on the conductivity and the observed resistive switching properties. At the early stages after thin film fabrication, we observed clear rectifying and hysteretic characteristics of *I-V* curves, however no measureable current was found after an 8 month period of time due to the re-oxygenation of the thin film samples under ambient conditions and the associated removal of oxygen vacancies. A representative comparison result of all BTO films is shown in the supplementary information (Figure S4). However, if the BTO films are deposited with suitable top electrodes[41] rather than a conductive AFM tip, oxygen vacancies could potentially be captured within the film and retained for prolonged resistive switching characteristics. Further investigations by implementations of top electrodes are needed in this system. In order to clarify these resistive switching properties, we carried out *I-V* curve measurements for different poling history of the investigated material, as shown in Figure 4a. (a): i) Normal *I-V* curve (-4V → +4V → -4V), ii) *I-V* curve (-4V → +4V → -4V) after taking an I-V curve (0V → +8V), iii) *I-V* curve (-4V → +4V → -4V) after taking an *I-V* curve (0V → -8V). These *I-V* curves show that

the highest current is seen after a bias sweep from 0 to +8V, whereas the lowest current is found after taking a bias sweep from 0 to -8V. Our results clearly show, following the same trend as Figure 2, that a high positive pre-poling voltage increases current levels, whereas the high negative pre-poling voltage almost suppresses the current completely. Based on these results, we can consider that oxygen vacancies sufficiently move to or away from the surface under high electric field, whereas the field-induced distribution of the vacancies is rather small under low electric field. This indicates that high electric field can function as a bias to control the oxygen vacancy distribution for switching between HRS and LRS whereas the low electric field can be used to read a current at a specific resistance state.

To further evaluate the resistance switching behaviour, we also investigated time-dependent conduction properties by measuring *I-V* curves over different time scales. Figure 4b shows *I-V* curves up to 4V bias with different bias ramping speeds (10, 100, 1000 ms/point for 200 points per curve) for the sample cooled under 50 µTorr, with the most oxygen vacancies. Before taking *I-V* curves with different bias ramping speeds, the sample was poled with +8V for switching it to LRS. As a result, the current read at -4V show that a high speed scan (10 ms/point) retains the increased current set by positive bias while a slow speed scan (1000ms/point) shows the extremely decreased current set by negative bias, indicating that the
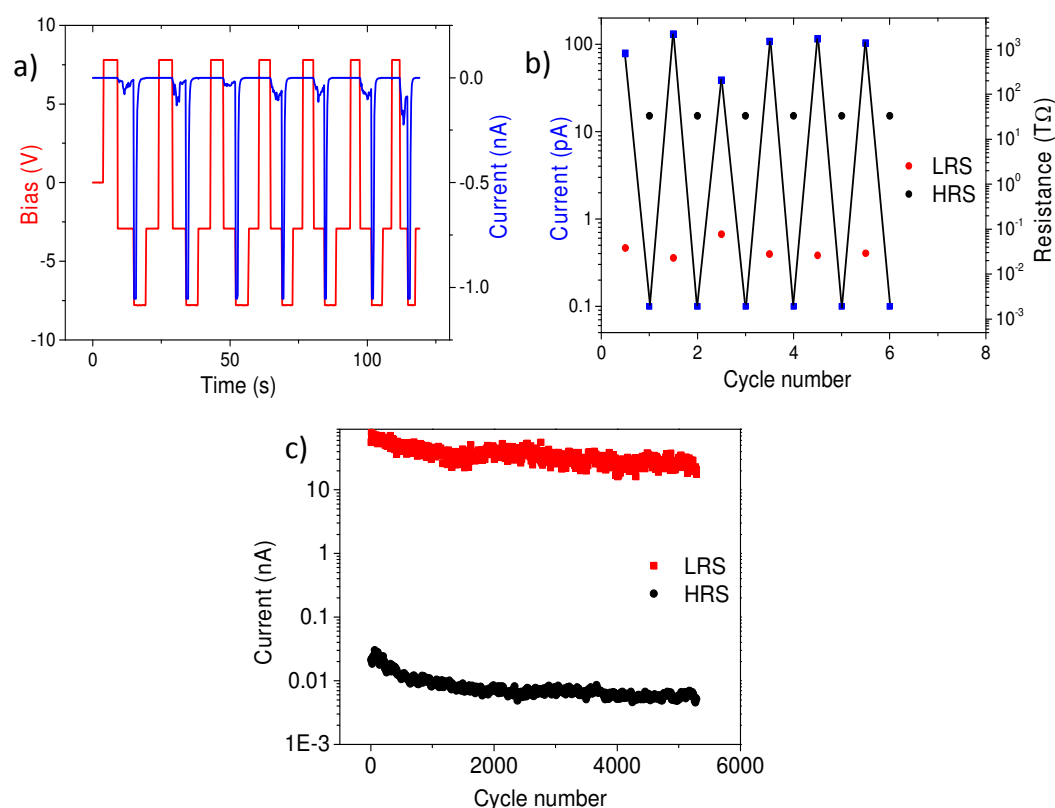
Figure 5. Pulse-voltage mode resistive switching behaviour. (a) Repeatability of the resistive switching behaviour of the 50 μTorr sample, measured in pulse-voltage mode. Pulsed bias voltages of ± 8V were respectively applied via conductive AFM tip. Switching voltages were alternated with a period of roughly 10 seconds. Resistance values were evaluated from mean current values at V = -3 V. The sequence of the applied voltages is shown in red and the resultant currents are plotted in blue. (b) The measured currents (blue squares) and the corresponding resistance (red and black circles) as a function of the number of the ± 8V bias voltage cycles. The current values were extracted from the plot in Figure 5a. Resistive switching of at least three orders of magnitude is observed (low resistance LRS vs. high resistance HRS state). (c) Pulse mode measurements for long cycles of *I-V* curves for 50 μTorr BaTiO$_{3-\delta}$ after additional heating in vacuum condition

resistance switching can be induced by adjusting the period of the applied bias. This can be attributed to time-varying dynamics of oxygen vacancies, which are known to be mobile and movable with electric fields.[51] Their diffusivity in certain perovskite oxides has been estimated to be of the order of 10^{-17} cm^2 s^{-1} at room temperature.[23] Our results offer promising aspects of resistive switching properties based on oxygen vacancies if strict control of the amplitude and period of the applied bias can lead to solid switching behaviour with little fatigue. In order to test the repeatability of the resistive switching, we explored pulsed-voltage-induced resistive switching characteristics, using a built-in oscilloscope in our AFM system. Figure 5 shows the resistive switching characteristics of the 50 μTorr sample. Pulsed bias voltages of ±8V are used in order to switch between high resistance state (HRS) and low resistance state (LRS). After switching with ±8V, -3V is used as a "read" voltage to evaluate conductivity by measuring current. Figure 5a shows the periodic resistive switching behaviour with pulsed bias voltages of ±8V over a 120 second period. After switching with +8V, currents

measured at -3V can be seen as a small trough and their average value is found to be around -100pA. On the other hand, after switching with -8V, current values read at -3V show almost no measurable current and are below the noise floor of our c-AFM system (~100fA). Moreover, we calculated resistance values using the measured currents at the -3V and plotted both values again the number of switching cycles. We found that the switching ratio (high resistance/low resistance) is greater than 10^3 as a lower limit based on mean HRS current values.

These results demonstrate the robustness of the bias-induced oxygen vacancy movements which are responsible for the switchable enhancement of the conductivity in BTO films as shown in Figure 3 (vacancies move to the film surface or away from the film surface).[23] To further evaluate the potential of our devices and test repeatability, we took long cycle pulsed mode measurements for testing the fatigue behaviour of resistive switching properties. We used a 50 μTorr BTO sample after heating it to 500°C for 10 minutes in vacuum conditions. To perform a data retention test, we applied up to 10^3 cycles of voltage stresses with a period of each cycle set as 8 seconds and

an amplitude of $V_p = \pm 8V$ for switching between LRS (+8V) and HRS (-8V), while current levels were instantaneously measured at -3V after switching. Our long time trace pulsed measurements show more than 650 cycles of resistive switching properties with little fatigue as shown in Figure 5c. In this case, the average switching ratio is found to be roughly ~4500. After more than 1000 cycles, the BTO still exhibited resistive switching characteristics with reduced currents read at LRS while the current level at HRS remained almost the same, thus giving a lower switching ratio. It is also interesting to note that the current level can be drastically modulated by the pulse duration time or amplitude of applied voltage, which in turn changes the switching ratio.

4. Conclusion

In summary, we have successfully deposited epitaxial oxygen deficient $BaTiO_{3-\delta}$ thin films on SRO buffered GSO substrates by pulsed laser deposition and following an after-growth oxygen cooling process, unveiled the resistive switching characteristics of these films with regard to underpinning mechanisms of such phenomena.[11, 52] These films show a clear resistive switching behaviour that is strongly dependent on the oxygen cooling pressures, resulting in the bias-induced modulation of oxygen vacancies in the system. Moreover, electrical poling can tune the resistance values by switching between HRS and LRS due to bias dependent movement of oxygen vacancies with the aid of formation of interfacial barriers. From a device perspective, our results demonstrate promising aspects for the use of oxygen deficient oxides tuned by after-growth oxygen cooling pressure treatments with ability to control resistive switching by electric field. Further investigations are needed to develop these devices and improve the degradation for memory applications.

Acknowledgements

References

1. A. I. Kingon, J.-P. Maria and S. K. Streiffer, *Nature*, 2000, **406**, 1032-1038.

2. Y. S. Kim, D. H. Kim, J. D. Kim, Y. J. Chang, T. W. Noh, J. H. Kong, K. Char, Y. D. Park, S. D. Bu, J.-G. Yoon and J.-S. Chung, *Applied Physics Letters*, 2005, **86**, 102907.

3. Y. W. Cho, S. K. Choi and G. V. Rao, *Applied Physics Letters*, 2005, **86**, 202905.

4. E. Y. Tsymbal and H. Kohlstedt, *Science*, 2006, **313**, 181-183.

5. A. Gruverman, D. Wu, H. Lu, Y. Wang, H. W. Jang, C. M. Folkman, M. Y. Zhuravlev, D. Felker, M. Rzchowski, C. B. Eom and E. Y. Tsymbal, *Nano Letters*, 2009, **9**, 3539-3543.

6. V. Garcia, S. Fusil, K. Bouzehouane, S. Enouz-Vedrenne, N. D. Mathur, A. Barthelemy and M. Bibes, *Nature*, 2009, **460**, 81-84.

7. M. Gajek, M. Bibes, S. Fusil, K. Bouzehouane, J. Fontcuberta, A. Barthelemy and A. Fert, *Nat Mater*, 2007, **6**, 296-302.

8. P. Maksymovych, S. Jesse, P. Yu, R. Ramesh, A. P. Baddorf and S. V. Kalinin, *Science*, 2009, **324**, 1421-1425.

9. S. Q. Liu, N. J. Wu and A. Ignatiev, *Applied Physics Letters*, 2000, **76**, 2749-2751.

10. A. Beck, J. G. Bednorz, C. Gerber, C. Rossel and D. Widmer, *Applied Physics Letters*, 2000, **77**, 139-141.

11. Y. Watanabe, J. G. Bednorz, A. Bietsch, C. Gerber, D. Widmer, A. Beck and S. J. Wind, *Applied Physics Letters*, 2001, **78**, 3738-3740.

12. A. Sawa, T. Fujii, M. Kawasaki and Y. Tokura, *Applied Physics Letters*, 2004, **85**, 4073-4075.

13. T. W. Hickmott, *Journal of Applied Physics*, 1962, **33**, 2669-2682.

14. I. G. Baek, M. S. Lee, S. Seo, M. J. Lee, D. H. Seo, D. S. Suh, J. C. Park, S. O. Park, T. I. Kim, I. K. Yoo, U. i. Chung and J. T. Moon, *Electron Devices Meeting, 2004. IEDM Technical Digest. IEEE International*, 2004, DOI: 10.1109/iedm.2004.1419228, 587-590.

15. B. J. Choi, D. S. Jeong, S. K. Kim, C. Rohde, S. Choi, J. H. Oh, H. J. Kim, C. S. Hwang, K. Szot, R. Waser, B. Reichenberg and S. Tiedke, *Journal of Applied Physics*, 2005, **98**, 033715.

16. K. Kinoshita, T. Tamura, M. Aoki, Y. Sugiyama and H. Tanaka, *Applied Physics Letters*, 2006, **89**, 103509.

17. D. B. Strukov, G. S. Snider, D. R. Stewart and R. S. Williams, *Nature*, 2008, **453**, 80-83.

18. R. Waser and M. Aono, *Nat Mater*, 2007, **6**, 833-840.

19. A. Baikalov, Y. Q. Wang, B. Shen, B. Lorenz, S. Tsui, Y. Y. Sun, Y. Y. Xue and C. W. Chu, *Applied Physics Letters*, 2003, **83**, 957-959.

20. L. L. Esaki, R.B.; Stiles, P.J, *IBM Technical Disclosure Bulletin* 1971, **13**, 2161.

21. P. W. M. Blom, R. M. Wolf, J. F. M. Cillessen and M. P. C. M. Krijn, *Physical Review Letters*, 1994, **73**, 2107-2110.

22. A. Schmehl, F. Lichtenberg, H. Bielefeldt, J. Mannhart and D. G. Schlom, *Applied Physics Letters*, 2003, **82**, 3077-3079.

23. R. Meyer, J. R. Contreras, A. Petraru and H. Kohlstedt, *Integrated Ferroelectrics*, 2004, **64**, 77-88.
24. L. Pintilie, V. Stancu, L. Trupina and I. Pintilie, *Physical Review B*, 2010, **82**, 085319.
25. M. P. Singh, L. Méchin, W. Prellier and M. Maglione, *Applied Physics Letters*, 2006, **89**, 202906.
26. S. Y. Wang, M. Li, W. F. Liu and J. Gao, *Physics Letters A*, 2015, **379**, 1288-1292.
27. S. C. Chae, J. S. Lee, S. Kim, S. B. Lee, S. H. Chang, C. Liu, B. Kahng, H. Shin, D.-W. Kim, C. U. Jung, S. Seo, M.-J. Lee and T. W. Noh, *Advanced Materials*, 2008, **20**, 1154-1159.
28. J. J. Yang, M.-X. Zhang, J. P. Strachan, F. Miao, M. D. Pickett, R. D. Kelley, G. Medeiros-Ribeiro and R. S. Williams, *Applied Physics Letters*, 2010, **97**, 232102.
29. J. J. Yang, D. B. Strukov and D. R. Stewart, *Nat Nano*, 2013, **8**, 13-24.
30. M. D. Pickett, D. B. Strukov, J. L. Borghetti, J. J. Yang, G. S. Snider, D. R. Stewart and R. S. Williams, *Journal of Applied Physics*, 2009, **106**, 074508.
31. D.-H. Kwon, K. M. Kim, J. H. Jang, J. M. Jeon, M. H. Lee, G. H. Kim, X.-S. Li, G.-S. Park, B. Lee, S. Han, M. Kim and C. S. Hwang, *Nat Nano*, 2010, **5**, 148-153.
32. J. P. Strachan, M. D. Pickett, J. J. Yang, S. Aloni, A. L. David Kilcoyne, G. Medeiros-Ribeiro and R. Stanley Williams, *Advanced Materials*, 2010, **22**, 3573-3577.
33. J. Blanc and D. L. Staebler, *Physical Review B*, 1971, **4**, 3548-3557.
34. R. Waser, T. Baiatu and K.-H. Härdtl, *Journal of the American Ceramic Society*, 1990, **73**, 1654-1662.
35. H.-I. Yoo, M.-W. Chang, T.-S. Oh, C.-E. Lee and K. D. Becker, *Journal of Applied Physics*, 2007, **102**, 093701.
36. D. Kan and Y. Shimakawa, *Applied Physics Letters*, 2011, **99**, -.
37. J. Shin, S. V. Kalinin, A. Y. Borisevich, E. W. Plummer and A. P. Baddorf, *Applied Physics Letters*, 2007, **91**, -.
38. M. L. Scullin, J. Ravichandran, C. Yu, M. Huijben, J. Seidel, A. Majumdar and R. Ramesh, *Acta Materialia*, 2010, **58**, 457-463.
39. C. H. Yang, J. Seidel, S. Y. Kim, P. B. Rossen, P. Yu, M. Gajek, Y. H. Chu, L. W. Martin, M. B. Holcomb, Q. He, P. Maksymovych, N. Balke, S. V. Kalinin, A. P. Baddorf, S. R. Basu, M. L. Scullin and R. Ramesh, *Nat Mater*, 2009, **8**, 485-493.
40. C.-H. Yang, D. Kan, I. Takeuchi, V. Nagarajan and J. Seidel, *Physical Chemistry Chemical Physics*, 2012, **14**, 15953-15962.
41. A. Ikeda-Ohno, J. S. Lim, T. Ohkochi, C. H. Yang and J. Seidel, *Physical Chemistry Chemical Physics*, 2014, **16**, 17412-17416.
42. S.-L. Li, J. Li, Y. Zhang, D.-N. Zheng and K. Tsukagoshi, *Appl. Phys. A*, 2011, **103**, 21-26.
43. P. Maksymovych, J. Seidel, Y. H. Chu, P. Wu, A. P. Baddorf, L.-Q. Chen, S. V. Kalinin and R. Ramesh, *Nano Letters*, 2011, **11**, 1906-1912.
44. J. Seidel, G. Singh-Bhalla, Q. He, S.-Y. Yang, Y.-H. Chu and R. Ramesh, *Phase Transitions*, 2012, **86**, 53-66.
45. T. Choi, S. Lee, Y. J. Choi, V. Kiryukhin and S.-W. Cheong, *Science*, 2009, **324**, 63-66.
46. M. Ben-Chorin, F. Möller and F. Koch, *Journal of Applied Physics*, 1995, **77**, 4482-4488.
47. L. Song-Lin, Z. L. Liao, J. Li, J. L. Gang and D. N. Zheng, *Journal of Physics D: Applied Physics*, 2009, **42**, 045411.
48. Y. A. Park, K. D. Sung, C. J. Won, J. H. Jung and N. Hur, *Journal of Applied Physics*, 2013, **114**, 094101.
49. J.-L. Gang, S.-L. Li, Z.-L. Liao, Y. Meng, X.-J. Liang and D.-M. Chen, *Chinese Physics Letters*, 2010, **27**, 027301.
50. A. Sawa, *Materials Today*, 2008, **11**, 28-36.
51. J. Seidel, W. Luo, S. J. Suresha, P. K. Nguyen, A. S. Lee, S. Y. Kim, C. H. Yang, S. J. Pennycook, S. T. Pantelides, J. F. Scott and R. Ramesh, *Nat Commun*, 2012, **3**, 799.
52. J. Rodríguez Contreras, H. Kohlstedt, U. Poppe, R. Waser, C. Buchal and N. A. Pertsev, *Applied Physics Letters*, 2003, **83**, 4595-4597.